JET–P(99)03

K D Lawson et al

# Impurity Transport in JET L-mode Discharges

JET–P(99)03

# Impurity Transport in JET L-mode Discharges

K D Lawson[1], L Lauro-Taroni, R Giannella[2],
N A C Gottardi[3], N C Hawkes[1], P D Morgan, M G O'Mullane[4],
N J Peacock[1], P Smeulders.

JET Joint Undertaking, Abingdon, Oxfordshire, OX14 3EA,UK.
[1]EURATOM/UKAEA Fusion Association, Culham Science Centre, Abingdon, Oxon, OX14 3DB, UK.
[2]Association EURATOM-CEA, CE Cadarache, 13108, Saint Paul lez Durance, France.
[3]Commission European Community, DGXVII, E2 Bâtiment Cube, L2920, Luxembourg.
[4]Dept. of Physics and Applied Physics, University of Strathclyde, 107 Rotten Row, Glasgow, G4 0NG, UK.

Preprint of a Paper submitted for publication in Nuclear Fusion

March 1999

**ABSTRACT**

The transport of intrinsic impurities has been studied in JET (Joint European Torus) L-mode discharges. The analysis reconsiders the question of the convective pinch in the plasma core, which was discussed by Giannella *et al*. (1994), and an investigation is made of the L-mode edge transport barrier, evidence for which was first presented by Denne-Hinnov *et al*. (1993).

The present study of three, 3.5MA, 3.4T limiter discharges with ~10MW RF additional heating analyses the radiation, including the VUV and XUV line emission from C and Ni, the only two significant impurities in these discharges. Use has been made of the empirical LINT method to derive elemental radiated power components of the impurities and impurity concentrations. The simulations have been carried out using the $1\frac{1}{2}$-D SANCO impurity transport code with atomic data taken from the ADAS data base. These results show that within experimental uncertainties the inward particle pinch in the bulk of the plasma is negligible and a linear dependence is found between the magnitude of the edge transport barrier and the diffusion coefficient in the outer region of the plasma. Both convective and diffusive barriers have been considered and, using a more precise definition for their magnitude than before, their relative effectiveness quantified. Since it is not possible to determine a unique value for the magnitude of the edge barrier or whether it has a convective or diffusive mechanism for the present intrinsic impurities, which only vary slowly with time, the analysis relating to the edge barrier is applied to the results of Denne-Hinnov *et al.* who were able to fix the size of the barrier for medium Z elements.

## 1. INTRODUCTION

In the fluid approximation, the cross-field impurity transport is conveniently described in terms of diffusive and convective components, which relate ion densities and their gradients to radial ion fluxes. The coefficients are most accurately determined from detailed simulations of the ion fluxes and two recent studies have led to improved understanding of these transport parameters for the bulk plasma in JET, L-mode discharges. Giannella *et al.* (1994) provide evidence of central transport that is slow compared to the anomalously high transport occurring in the outer regions of the plasma and give parameter scans over a wide range of the L-mode operating domain of JET, in particular discussing the role of the current profile; Denne-Hinnov *et al.* (1993) demonstrate the need for a transport barrier at the plasma edge, within a few per cent of the normalized minor radius from the Last Closed Flux Surface (LCFS). Both studies involve analyses of transient medium or high Z impurities, such as Fe, Ni and Ag, injected into the plasma by a laser ablation system (Magyar *et al*. 1988).

An alternative approach is to determine the transport parameters from the more slowly varying impurities intrinsic to the plasma. Such an analysis has been made for limiter, L-mode discharges run during a high power ICRH (Ion Cyclotron Resonance Heating) campaign on JET in December 1987. The exceptionally high level of the medium Z element Ni in these pulses

ensures a high degree of confidence not only in the measurements relating to this element, but also for the other intrinsic impurity in these discharges, which is C. Passive line radiation from Ni is emitted from a wide spatial extent within the plasma, making this element ideal for this investigation.

Impurity transport modelling is highly complex, involving the solution of the continuity equations to give ion density profiles, the use of atomic physics data and requiring the validation of a number of experimental observations, for which there can be significant uncertainties particularly towards the plasma edge. Use is therefore made of a novel, empirical technique, the LINT (Line Integration Normalization Technique) procedure (Lawson *et al*. 1998), to provide additional constraints on the simulations. The LINT method has been employed on the JET tokamak to provide routine information about the elemental radiated power components and concentrations of intrinsic impurities in the bulk of the plasma. This is achieved by normalizing XUV and VUV spectral line intensities measured along a near horizontal line of sight to the total radiated power and to the effective ion charge, $Z_{eff}$. The technique essentially converts the line of sight intensities into global parameters using the absolute calibration of the bolometers and visible bremsstrahlung spectrometer from which the $Z_{eff}$ is derived. It has been extensively applied to JET limiter discharges.

The transport simulations have been carried out using the $1\frac{1}{2}$-D SANCO impurity transport code (Lauro-Taroni *et al.* 1994), which in turn uses atomic data from the ADAS (Atomic Data and Analysis Structure) data base (von Hellermann and Summers 1993). The simulations are optimized to give the best possible agreement with all the available experimental data and are described in the next section, together with details of the measurements used. In section 3, the results of this modelling are discussed. The pinch or convection term in the bulk of the plasma is assessed and an investigation of the edge transport barrier is made. Both convective and diffusive barriers are studied and their relative importance determined. In the present analysis, it was not possible to determine reliably the magnitude of the edge barrier and so a comparison is made with the results of the laser ablation experiment of Denne-Hinnov *et al.*

## 2. THE TRANSPORT SIMULATIONS

Transport simulations have been carried out for three, L-mode, limiter discharges chosen from a sequence of 3.5MA, 3.4T pulses in a high power, ICRH campaign. At this time, the plasma facing surfaces were C tiles, Ni ICRH antenna screens and the Inconel vessel walls. The use of ICRH with monopole phasing resulted in significant levels of Ni entering the plasma from the antenna screens. Consequently, the main impurities were C and Ni, the latter when redeposited on plasma facing surfaces being so important as to getter O to the extent that it was no longer a significant contaminant. The discharges studied, pulses 13728, 13734 and 13738, have D fuel with a $^3$He minority, which allowed between 9 and 10MW of ICRH power to be coupled to the plasma. The Ni levels were particularly high in pulse 13738, resulting in the plasma disrupting at 9s.

The analysis is made for times when the ICRH power is close to maximum and remains approximately constant. Since sawteeth can lead to a redistribution of particles within the core of the plasma, care was taken to use sawteeth-free periods of the discharge. The periods used are listed in table 1 together with some pertinent plasma parameters and time histories of these parameters are shown for pulse 13738 in figure 1.

*Table 1. Plasma parameters of the pulses studied.*

| Pulse number | 13728 | 13734 | 13738 |
|---|---|---|---|
| Time of simulation (s) | 9 - 10 | 8 - 10 | 7 - 9 |
| Plasma Current (MA) | 3.5 | 3.5 | 3.5 |
| Maximum $T_e$ (keV) | 10.3 | 12.0 | 11.0 |
| Maximum $n_e$ ($m^{-3}$) | 4.0 x $10^{19}$ | 3.8 x $10^{19}$ | 4.6 x $10^{19}$ |
| ICRH Power (MW) | 9.0 | 10.0 | 9.7 |
| Stored Energy (MJ) | 3.5 | 5.1 | 4.6 |
| Radiated Power (MW) | 4.8 | 5.4 | 6.2 - 8.1 |
| $Z_{eff}$ | 5.5 | 6.2 | 5.3 - 5.7 |

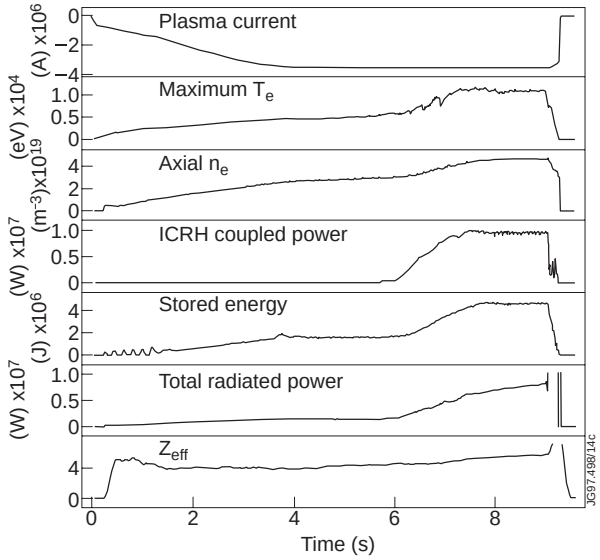


*Fig.1. Time histories of the main plasma parameters for pulse 13738, their magnitude being typical of the modelled discharges. Pulse 13738 disrupts at 9s due to the high Ni levels.*

Simulations of intrinsic impurities are usually restricted by the necessity of making comparisons with the total radiated power, $P_{rad}$, and often with the effective ion charge, $Z_{eff}$. In the present case, individual elemental components of the radiated power and the contributions of each element to the $Z_{eff}$ have been derived using the LINT empirical procedure, the $Z_{eff}$ contributions allowing the impurity concentrations to be derived. The presence of only two significant impurities in these discharges makes the application of the LINT method to these pulses particularly reliable. The components are illustrated for pulse 13738 in figure 2 and the good agreement seen in this figure between the components' sums and the total $P_{rad}$ and $Z_{eff}$ is found for all three pulses. The accuracy of the $P_{rad}$ components is estimated to be ±15% and that of the concentrations to be ~30%, thus putting additional stringent constraints on the transport analysis.

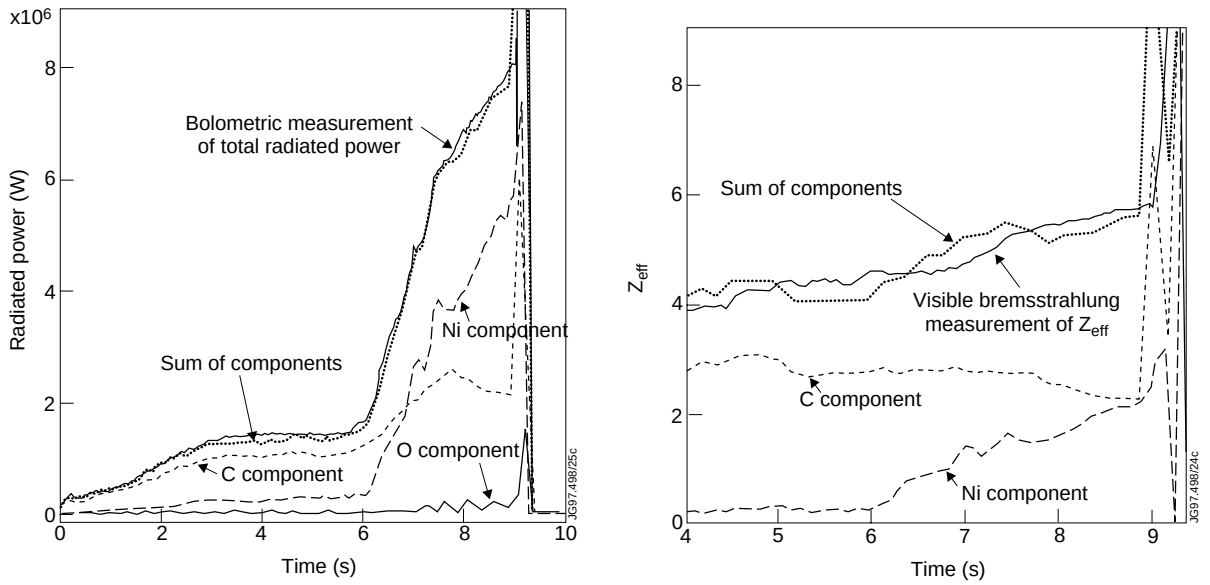


*Fig.2. a) Elemental $P_{rad}$ components derived from the LINT method, the components' sum and the total radiated power and b) the measured $Z_{eff}$ and its empirically derived elemental contributions, together with their sum for pulse 13738.*

### 2.1. The experimental techniques

Although all available observations have been compared with the transport simulations, the greatest weight has been given to line-of-sight integrated spectral line intensities, since their calculation is considered to be the most reliable. The Ni spectral lines were recorded with a VUV, McPherson-Schoeffel spectrometer (Fonck *et al*. 1982), which viewed the plasma via a gold-coated mirror. This instrument has a holographic, toroidal diffraction grating which results in a flat focal field and, with the 450g.mm$^{-1}$ grating employed in these experiments, observes a wavelength range of ~100 to 1100Å. This range includes C lines belonging to low ionization stages, but the CV and CVI resonance lines fall at shorter wavelengths, ~30 to 40Å, for which an XUV, grazing incidence, Schwob-Fraenkel spectrometer was used (Schwob *et al*. 1987). No sensitivity calibration was available for the latter instrument. Lawson *et al*. (1987) give an absolute calibration for the VUV instrument, although a modification at the shortest wavelengths, below 150Å, was required to account for a loss of reflectivity that had occurred over a period of time due to the degradation of the mirror surface. The accuracy of the absolute calibration is estimated to be better than ±40%.

The bolometric measurements were made with one vertical and two horizontal pinhole cameras, situated at one toroidal location and viewing the whole of one poloidal cross-section, and eight single bolometers used to monitor the toroidal symmetry of the plasma emission (Mast *et al*. 1985). The vertical camera was used to determine the total power radiated from the plasma. The bolometers are sensitive to both radiation and particles, but estimates of the neutral particle fluxes (Bracco *et al*. 1991) showed that their contribution was small (less than a few per cent) compared to that of the radiation in the pulses of interest.

Electron density, $n_e$, and temperature, $T_e$, profiles are used both as input to the transport simulations and in the calculation of the effective ion charge of the plasma. These were routinely available, respectively, from measurements of a 7 channel interferometer operating in the far infrared at a wavelength of 195μm (Braithwaite *et al*. 1989) and from an Electron Cyclotron Emission (ECE) Michelson interferometer (Bartlett *et al*. 1987). Measurements from a high temporal resolution, ECE grating polychromator (Bartlett *et al*. 1987) gave information about fast events, such as sawteeth.

A spatially averaged value of the effective ion charge of the plasma, $Z_{eff}$, was determined from the radiance, ε, as measured in the continuum of the visible spectral region at a wavelength of 5235±5Å observed along a vertical line of sight,

$$Z_{eff} = \frac{c\varepsilon}{2\int_0^1 n_e^2(x)\, T_e^{-0.5}(x)\, dx},$$

where c is a constant and x the normalized minor radius (Morgan and O'Rourke 1987).

In addition to spectral line intensities, $P_{rad}$ components and concentrations, radial profiles of the soft X-ray emission were available and were compared with the results of the simulations. These profiles were derived from measurements recorded with two, soft X-ray 'pinhole cameras', made up of arrays of silicon diode detectors (Edwards *et al*. 1986). One of the cameras has a horizontal view, the other a vertical view, this covering a complete poloidal cross-section of the plasma and allowing the soft X-ray profiles to be constructed. A 250μm, Be filter was used in the cameras resulting in ~2.0keV low energy cut-off.

### 2.2. The transport code

The transport simulations have been carried out using the 1½-D, time-dependent SANCO impurity transport code (Lauro-Taroni *et al*. 1994). Employed widely for the analysis of JET data, this code takes account of the plasma geometry by reducing the variables to magnetic surface averages. In the fluid approximation, the radial flux of impurities is described as the sum of a diffusive and convective term for each ionization stage Z,

$$\Gamma_Z(r,t) = -D(r)\nabla n_Z(r,t) + V(r)n_Z(r,t),$$

where D(r) and V(r) are radial profiles of the diffusion coefficient and convection velocity, for these simulations assumed constant in time, and $n_Z(r,t)$ is the particle density. The convention that a positive V(r) indicates an outward velocity is adopted.

In the simulation, two calculations depend on atomic physics data; these are taken from the ADAS data base (von Hellermann and Summers 1993). The first involves the use of ionization, $S_Z$, and recombination rates, $\alpha_Z$, in the source term of the continuity equations,

$$\frac{\partial}{\partial t} n_Z(r,t) + \nabla\Gamma_Z(r,t) = -S_Z n_Z(r,t) + S_{Z-1} n_{Z-1}(r,t) - \alpha_Z n_Z(r,t) + \alpha_{Z+1} n_{Z+1}(r,t),$$

which are solved for each ionization stage to give radial profiles of the particle densities. Secondly, atomic data is employed in calculations of the power radiated by specific spectral lines and the total power radiated by each ionization stage, the latter including line radiation, recombination radiation and bremsstrahlung. The total power for each stage is summed for all stages to give the power radiated by the element. In addition, allowance is made for the transmission of the soft X-ray filter used, so as to permit comparisons with the measured soft X-ray profiles.

Frictional forces between the impurities were neglected, the simulations for each element being carried out independently.

### 2.3. The simulations for C

The high electron temperatures found in JET ($T_{emax}$ ~2-15keV) result in the passive C line emission originating from close to the plasma edge, where uncertainties in the $T_e$ and $n_e$ profiles are largest. In addition, the resonance C lines emitted from within the LCFS are observed with the XUV spectrometer, for which there is no independent sensitivity calibration. The accuracy of the transport modelling for the C impurity is therefore limited. Nevertheless, the simulations prove useful in two important respects. They indicate the need for an edge transport barrier and enable the contribution made by C to the soft X-ray emission to be determined. The latter is required to allow comparisons with the measured soft X-ray emission, which is due to both Ni and C.

The influx of C, which must be specified in the simulation, is normalized to give agreement with the empirically derived LINT C concentration and the spectrometer sensitivity calibration is then found from a comparison of the simulated and measured CVI spectral line intensities. In determining the concentrations by the empirical LINT method, a line of sight averaged measurement of the $Z_{eff}$ was used. The emission from which this is calculated depends on the integral $\int n_e^2(r)\, T_e^{-0.5}(r)\, dr$ and the derived concentration is therefore biased to the plasma region where the integrand of this function is large. In these pulses, the integrand was found to be slowly varying within a normalized minor radius of $x < 0.6$, falling away more steeply outside this region. Consequently, the empirically derived concentration applies to this inner region of plasma. The normalization to the concentration therefore ensures the most accurate calculation of the C soft X-ray component, since the concentration is appropriate to the plasma region from where the soft X-rays are emitted. This minimizes the sensitivity of the calculated soft X-ray contribution to transport effects.

To find agreement with the measured CV spectral line intensity, it was necessary to reduce the simulated value by introducing a transport barrier at the plasma edge, the CV emission straddling the LCFS. The introduction of this barrier is consistent with the results of Denne-Hinnov *et al*. (1993), who use a combination of a diffusive and convective barrier, and with the analysis by Giannella *et al*. (1994) of 7MA discharges. In the present study, the best agreement was obtained by also modifying the outer $n_e$ and $T_e$ profiles, for $x > 0.7$. Such a modification was

considered, because of the uncertainties in these profiles close to the plasma edge. It follows that a precise determination of the magnitude of the edge transport barrier, which is defined in section 3, is unreliable. Neither is it possible to distinguish between a diffusive and convective barrier in these pulses, in which the bulk parameters are slowly varying. In the simulations for Ni, a range of both diffusive and convective barriers has been studied.

### 2.4. The simulations for Ni

In contrast to the passive line emission from C, spectral line emission from a medium Z element such as Ni is radiated from all spatial locations within the bulk plasma, allowing radial profiles of the transport parameters for these elements to be determined. When making comparisons between the simulations and measurements, particular emphasis was given to the line of sight integrated spectral line intensities, since their calculation is expected to be more reliable than those of total powers. Five Ni spectral lines are observed in the spectral region between ~160 and 330Å, where the sensitivity calibration of the VUV instrument is only slowly varying. This ensures a higher accuracy for the relative sensitivity calibration of these lines, better than ±20%, than for the absolute calibration of ±40%. Particular use is made of the near-coincidence in the spectrum of two features, the NiXXVI 234Å and NiXVII 249Å lines. Their proximity in the spectrum ensures a relative calibration accuracy of about ±10%, despite the emission originating from different regions of the plasma, as is illustrated in figure 3. For the Ni simulations, the particle influx was determined by normalizing to the line of sight measurement of the NiXVII line intensity, this line belonging to the outermost ionization stage observed.

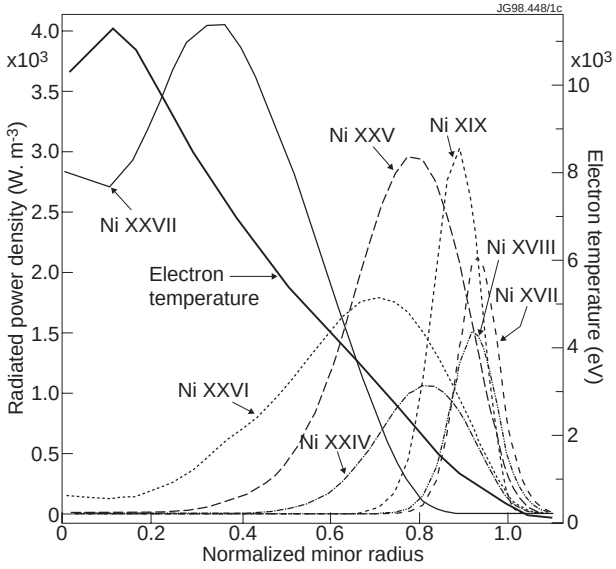


*Fig.3. Radial profiles of $T_e$ and the simulated Ni line emissions for the ionization stages neighbouring NiXVIII and NiXXVI at 8.0s in pulse 13738, showing that the observed line emission originates largely from the outer region of the plasma.*

Unlike the total radiated power, for which the LINT method is used to derive C and Ni components, no division of the soft X-rays into their component parts is possible. The C contribution to the soft X-rays is found to be typically between 10 and 30%, if the same transport is assumed for both elements. The effect of uncertainties in the C component is therefore smaller than in the case of Ni.

Simulations were made for a range of transport parameters, as described in the next section, and examples of comparisons with the experimental data are given in table 2. These data apply to cases when a convective edge transport barrier is used. Use of a diffusive edge barrier

lowers the ratio of the measured to simulated radiated powers by between 4 and 10%. Generally, agreement within the expected errors is found for the line intensities, concentrations and central values of the soft X-ray emission and, given the complexity of the modelling and the uncertainties associated with the experimental measurements, the simulations are regarded as being very satisfactory.

*Table 2. Examples of ratios of the measured (including the empirically determined concentrations and $P_{rad}$) to simulated line intensities, concentrations and powers for each of the pulses studied.*

| Pulse number | 13728 | 13734 | 13738 |
|---|---|---|---|
| Outer D ($m^2.s^{-1}$)* | 2 | 3 | 5 |
| $\int_0^1 (x-0.96)^2 V(x)dx \left(m.s^{-1}\right)^+$ | -2.64 x $10^{-4}$ | -4.43 x $10^{-4}$ | -8.35 x $10^{-4}$ |
| Line Intensities | | | |
| NiXVII – 249Å | 1.00 | 1.00 | 1.00 |
| NiXVIII – 292Å | 1.07 | 1.26 - 1.28 | 0.99 - 1.06 |
| NiXVIII – 321Å | 1.10 | 1.19 - 1.20 | 1.13 - 1.19 |
| NiXXV – 118Å | 0.97 | 0.94 - 1.10 | 0.84 - 0.92 |
| NiXXVI – 165Å | Detector saturating | Detector saturating | 0.87 - 0.92 |
| NiXXVI – 234Å | 0.92 | 0.87 - 1.07 | 0.87 - 1.00 |
| Ni Concentration# | 0.79 | 0.63 - 0.78 | 0.78 - 0.79 |
| Ni Radiated Power | 1.37 | 1.15 - 1.38 | 1.31 - 1.32 |
| Soft X-rays | | | |
| x=0.1 | 0.92 | 0.90 - 0.95 | 0.73 - 0.77 |
| x=0.6 | 0.61 | 0.55 - 0.65 | 0.47 - 0.54 |

*The adopted value of the diffusion coefficient for a normalized radius x > 0.4.
+The term for the convective edge transport barrier, whose magnitude is derived from the simulations, is discussed in section 3.
#An averaged ratio of the total Ni ion to electron density for x < 0.6.

There are two discrepancies of note. The simulations overestimate the soft X-ray emission away from the plasma centre and tend to underpredict the total radiated power due to Ni, especially when a convective edge barrier is used. No simple adjustment can be made to remove these discrepancies, since the errors are in opposite directions and the peak of the total radiation and the largest discrepancy in the soft X-rays occur at radii close to the centre of the NiXVII and NiXXVI emission regions. This is evident from a comparison of figures 3 and 4, the latter figure showing radial profiles of the soft X-ray and total emissions.

Consideration was given to possible sources of error which might explain these discrepancies including uncertainties in the spectrometer sensitivity calibration, spatial asymmetries in the emitted radiation and unaccounted radiation from the scrape off layer (SOL), the SANCO code describing the transport within the bulk plasma, with only a simplistic representation of the complex transport within the SOL, which requires a 2D treatment. None of these possibilities satisfactorily explain the discrepancies.

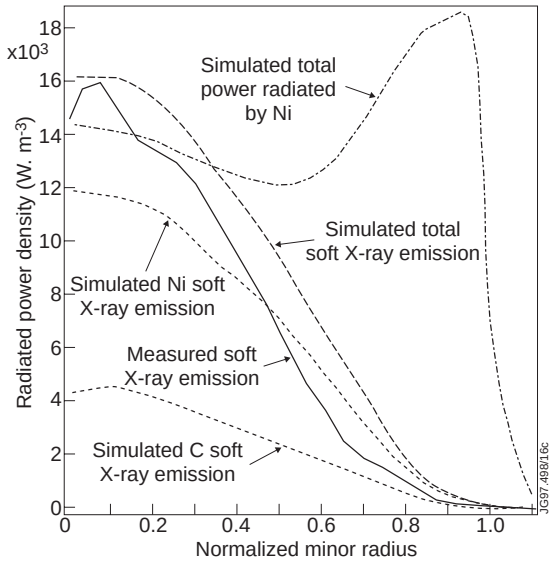


*Fig.4. Radial profiles of the measured and simulated soft X-ray emissions and of the simulated total power radiated by Ni at 8.5s in pulse 13734. The total power peaks close to the radii of the NiXVII emission shell (figure 3), whereas the largest discrepancy in the measured and simulated soft X-ray emission coincides with the region of the NiXXVI line emission.*

Given the uncertainties in the outer $T_e$ and $n_e$ profiles, these were varied outside x ~ 0.7. Significant changes to the profiles did lead to some reduction in the radiated power discrepancy, although not its complete removal. However, changes that helped to reduce the discrepancy in $P_{rad}$ tended to increase that with the soft X-rays or were inconsistent with the changes required to give the best C simulations.

When calculating the radiated power using ADAS, the contribution of the line radiation is determined separately from the contribution due to recombination radiation and bremsstrahlung. For the total power the component due to line radiation is both larger and involves contributions from more ionization stages than for the soft X-ray emission. The Be filter used to discriminate against low energy radiation ensures that it is mainly the Li-like and higher stages that contribute to the latter, the atomic data being most reliable for these stages. The discrepancy in $P_{rad}$ may indicate a limitation in the atomic data used for the line radiation of the lower Ni ionization stages, such as NiXV to NiXXV.

Agreement is found for the central soft X-rays, but not for the whole of the soft X-ray profile, the measured profile always falling away more rapidly than can be explained by the simulations. No satisfactory explanation has been found and this brings into question the reconstruction of the measured profile for these pulses. A more detailed discussion of the sources of the errors is presented by Lawson *et al*. (1998).

## 3. DISCUSSION

The radial profiles of the transport parameters used were based on those of Giannella *et al*. (1994). The diffusion coefficient, D(r), has a high value in the outer region of the plasma, $D_{out}$, corresponding to an anomalous transport process and there is an inner region of low transport, with a coefficient close to that expected of a neoclassical mechanism, as illustrated for pulse 13728 in figure 5. The available magnetic data for the present pulses suggests that the safety factor is similar to those of the 3 and 4MA pulses investigated by Giannella *et al*. and, consequently, the radius of the transition shell between the outer anomalous and inner low transport regions was positioned, consistent with their results, at a normalized minor radius of 0.3 to 0.4. In the present discharges, the impurity levels are slowly varying and changes to the inner diffu-

sion coefficient had no effect on the parameters compared with the available experimental data; consequently, an inner diffusion coefficient of ~0.1$m^2.s^{-1}$ was used for all the simulations. The simulations proved most useful in determining the transport in the outer region of the plasma, even being relatively insensitive to the radial position of the transition shell. After some initial checks, this shell was fixed at x ~0.3 to 0.4. Various modifications to the shape of the outer D(r) were tested, but no justification was found for using anything other than a flat outer profile for D(r). A range of transport was studied by selecting 5 different values for the outer D(r), from ~1 up to an extreme case of 5$m^2.s^{-1}$, the resulting profiles being represented by the different curves in figure 5.

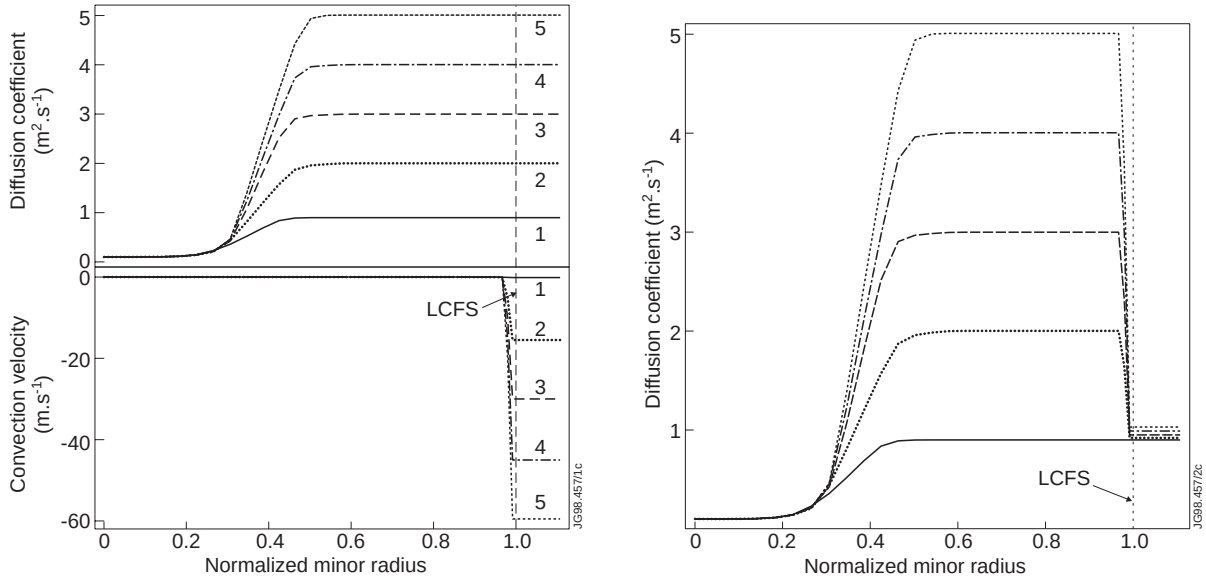


*Fig.5. Radial profiles of the transport parameters, D(r) and V(r), used in simulations for pulse 13728 a) with a convective and b) with a diffusive edge transport barrier. The labelling in a) is the outer value of D and indicates the corresponding D(r) and V(r). For case b) the edge barrier is due entirely to the reduction in D just inside the LCFS to ~1$m^2.s^{-1}$, V(r) (not shown) being negligible over the whole profile.*

The convective velocity used by Giannella *et al*. (1994) is of the conventional form, together with a peaking factor, S,

$$V(r) = -2S\,\frac{D(r)\,r}{a^2},$$

where a is the minor radius at the LCFS. A value of S = 1 was employed in the majority of their simulations. Such a convective term gives too strong an inward particle flux in the present study, the most satisfactory agreement between the simulations and experiment being found with no significant convection away from the plasma edge.

As a consequence of the modelling of C, an edge transport barrier was used in the simulations for Ni. The emission shell of the outermost Ni ionization stage observed, NiXVII, falls largely inside the proposed barrier, but, despite this, the barrier has a significant effect on the transport within the bulk of the plasma, affecting the balance of confined particles. A high diffusion coefficient tends to exhaust particles from the plasma, whereas the edge barrier has the effect of

containing the impurity particle inventory. A consequence of the observed emission coming from within the edge barrier is that it is not possible either to determine a unique value for the magnitude of the barrier or to distinguish between a convective and diffusive mechanism. Nevertheless, the requirement of particle balance ensures a correlation between the chosen outer D(r) and the barrier magnitude. Both convective (figure 5a) and diffusive (figure 5b) barriers were studied. In figure 5a, the labels indicate the corresponding profiles of the diffusion coefficient and convection velocity.

Since an inward convection velocity in the plasma bulk has the effect of containing particles, the interrelation of a core pinch with the edge transport barrier must be considered. A finite value of S, the convective term peaking factor, offsets the need for an edge transport barrier. The maximum value of S corresponds to no edge barrier and, say for an outer D of $5m^2.s^{-1}$, S is found to be at the very most ~0.5. This maximum value of S corresponds to the lower end of the range given by Wesson (1997). In fact, the present simulations do allow discrimination between the use of a finite S and an edge transport barrier. When S is finite, the discrepancies for the radiated power and line intensities increase, in particular the discrepancy for the 234Å NiXXVI line rising to ~35%. Since the normalization to fix the influx is to the neighbouring 249Å NiXVII line, this discrepancy should not exceed ~10%. It follows that, whether or not an edge transport barrier is used, the preferred value of S in this modelling is ~0. Its precise value, whether it is exactly 0 or just small, is subject to the various uncertainties in the experimental and atomic data. In either case, the radial profile of the ion density will be nearly flat, leading to hollow concentration profiles in these pulses, which have peaked $n_e$ profiles. In the simulations investigating the edge transport barrier, the particular case of S = 0 is considered.

When defining the magnitude of a convective edge barrier, it is insufficient simply to take the convection velocity at the LCFS, since a barrier with a wider profile is better at containing particles than one with a narrow profile. Empirically, the integral $\int_0^1 (x-0.96)^2 V(x)\,dx$ is found to account satisfactorily for the width of the barrier, in that barriers with the same value of this integral confine particles to the same extent as is shown by them requiring the same outer diffusion coefficient; this expression is therefore used to define the magnitude of a convective barrier. In this integral, the zero is displaced to x = 0.96, which is the peak of the NiXVII ion density profile. It should be noted that none of the experimental measurements used had a high spatial resolution near the plasma edge. Consequently, the width of the barrier as defined above is largely a feature of the SANCO modelling and, in particular, of the profile of the NiXVII ion emission, rather than having any physical significance.

The diffusive barrier, illustrated in figure 5b, is much less sensitive to changes in its profile, behaving more like a wall over which the particles must ‘climb’. In this case a small correction is made to the magnitude of the barrier, $(D_{out}-D_{LCFS})$, where $D_{LCFS}$ is the diffusion coefficient at the LCFS. This magnitude, essentially the drop in the diffusion coefficient from its outer

level, $D_{out}$, is empirically found by requiring the barrier always to confine particles to the same extent and is

$$D_{diff} = (D_{out} - D_{LCFS}) + \left(\frac{5.31}{D_{out}}\right)\int_{0.8}^{1}(D_{out} - D(x))\,dx.$$

For both types of edge barriers a linear relationship is found between the magnitude of the barrier and $D_{out}$,

$$D_{out} = K_{con}\int_{0}^{1}(x - 0.96)^2 V(x)\,dx + D_{0con}$$

and

$$D_{out} = K_{diff} D_{diff} + D_{0diff}$$

for the convective and diffusive cases, respectively. These are illustrated in figure 6, the constants K and $D_0$ being given in table 3. Both intercepts, $D_{0con}$ and $D_{0diff}$, are ~1 and therefore can be cancelled when the equations are combined to give a mean relationship between the gradients of

$$K_{con} \approx -4240\,K_{diff}.$$

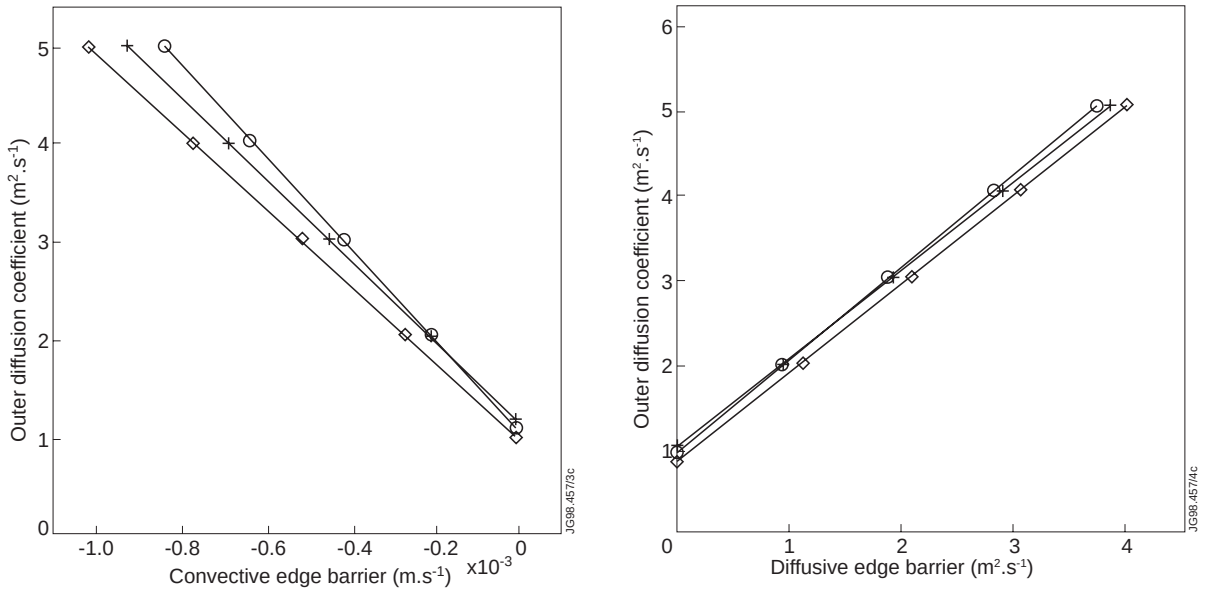


*Fig.6. Relationship between the outer diffusion coefficient and the magnitude of a) the convective and b) the diffusive edge transport barrier, for pulses 13728 (◊), 13734 (+) and 13738 (o). The good linear fits suggesting small statistical errors result from requiring the same balance of agreement and disagreement in all simulations.*

It should be noted that the small statistical errors evident in figure 6 result from the same balance of agreement and disagreement being required in all of the simulations, the linear form of the relationship as a consequence being relatively insensitive to experimental uncertainties. The investigation of the edge barriers in the present pulses was completed by confirming that, when used together, the effect of the convective and diffusive barriers is additive.

*Table 3. Values of the parameters defining the linear relationship of the particle balance.*

| Pulse number | 13728 | 13734 | 13738 |
|---|---|---|---|
| $K_{con}$ (m) | -4040 | -4270 | -4810 |
| $D_{0con}$ ($m^2.s^{-1}$) | 0.91 | 1.09 | 1.00 |
| $K_{diff}$ | 1.02 | 1.01 | 1.07 |
| $D_{0diff}$ ($m^2.s^{-1}$) | 0.87 | 1.04 | 0.97 |

Since, in the present study, it has not been possible to determine uniquely the magnitude of the edge transport barrier, the analysis has been applied to the results of Denne-Hinnov *et al*. (1993), who, in laser ablation experiments, were able to define a unique barrier. They present two simulations for a 3.5MA, 2.8T X-point discharge with 7MW of neutral beam heating. This contrasts with the present 3.4T limiter discharges, in which the 9 to 10MW of additional heating is ICRH. Their simulation A is consistent with the present study in having S ~ 0 in the bulk plasma, while their simulation B uses a core pinch term with S ~ 1 in addition to an edge barrier, as is shown in figure 7. The latter transport parameters would lead to inward particle fluxes several times larger than expected from the present analysis and, therefore, simulation B has not been included in the comparison. In their simulation A, Denne-Hinnov *et al*. find $D_{out}$ to be ~$2m^2.s^{-1}$ and they use a combined diffusive and convective barrier, which is equivalent to a diffusive barrier of $2m^2.s^{-1}$. This should be compared with an edge barrier of ~$1m^2.s^{-1}$, which from the present modelling would be expected for a $D_{out}$ of $2m^2.s^{-1}$ (figure 6b). Given the differences in toroidal field, configuration and heating regime and power, the closeness of these results is regarded as confirmation of the validity and usefulness of the main features of the present analysis.

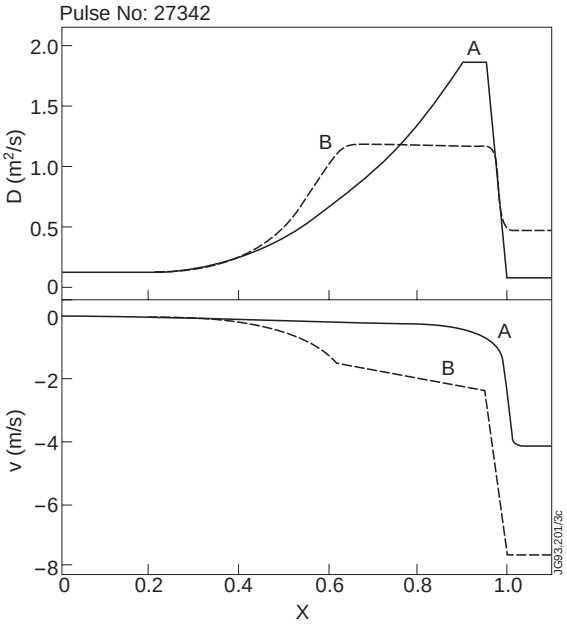


*Fig.7. Radial profiles of the transport parameters used in simulations A and B of Denne-Hinnov* et al. *(after Denne-Hinnov* et al. *1993). Simulation A has a negligible convection away from the plasma edge, as is found in the present modelling, whereas B has a convective term* $\sim \frac{2Dr}{a^2}$.

In a further application of this analysis, the relative importance of the diffusive and convective components of the edge barrier of Denne-Hinnov *et al*. can be judged. In fact, the barrier for simulation A is found to be 90% diffusive and only 10% convective, this being consistent with their observation that their data could also be fitted by reducing D(r) near the edge, while,

at the same time, keeping V(r) very small everywhere. It follows that their comparison of the convective velocity alone with the velocities of the edge transport barrier in H-mode discharges is inappropriate. Their analysis implies a diffusive edge transport barrier for L-mode discharges, this contrasting with the convective barrier found for H-mode plasmas (Giannella *et al*. 1989).

## 4. CONCLUSION

The impurity transport in JET L-mode discharges has been investigated by modelling the passive emission from the intrinsic impurities, C and Ni, in three limiter discharges chosen from an ICRH campaign. Additional constraints to the simulations were provided by the application of the LINT method, which enabled concentrations and $P_{rad}$ components for the individual impurities to be derived. The simulations were carried out using the $1\frac{1}{2}$-D, diffusive-convective SANCO impurity transport code, which takes atomic data from the ADAS data base.

In contrast to the results of Giannella *et al*. (1994), who analyse laser ablation experiments in a number of L-mode discharges and who find a significant core pinch term, the most satisfactory agreement in the present modelling uses transport parameters of which the convection term is negligible throughout the bulk of the plasma. Allowing for uncertainties in the experimental measurements and atomic data, a very small pinch (S ~ few per cent) would still be consistent with the observed data. The consequence is nearly constant radial profiles of the ion density and hollow concentration profiles.

The simulations for C provide evidence of an edge transport barrier, as is also required by the modelling of Denne-Hinnov *et al*. (1993). In the present case, however, its magnitude cannot be uniquely determined. The Ni simulations enable both diffusive and convective edge barriers to be studied, a linear relationship being found between the magnitude of the edge barrier and the diffusion coefficient in the outer region of the plasma. The relative strength of the two types of barrier was found and their additive effect when used together confirmed. Denne-Hinnov *et al*. were able to determine a unique magnitude for their edge barrier and the application of the present analysis to their simulation with no core pinch gave agreement to within a factor of 2. The combined convective and diffusive edge barrier of Denne-Hinnov *et al*. is shown to be almost entirely (90%) diffusive. This comparison confirms the validity of the diffusive-convective model and demonstrates the value of the present analysis.

## ACKNOWLEDGEMENTS

We would like to thank Drs. K Guenther, L D Horton and A C Maas for useful discussions. This work is partly funded by UK DTI and EURATOM.

**REFERENCES**

DENNE-HINNOV, B., *et al*., Proc. 20th EPS Conf. on Controlled Fusion and Plasma Physics, Lisboa, **I** (1993) 55

GIANNELLA, R., *et al*., Proc. 16th EPS Conf. on Controlled Fusion and Plasma Physics, Venice, **I** (1989) 209

GIANNELLA, R., *et al*., Nuclear Fusion, **34** (1994) 1185

VON HELLERMANN, M. G., and SUMMERS, H. P., 'Atomic and Plasma-Material Interaction Processes in Controlled Thermonuclear Fusion', Ed: Janev R K and Drawin H W, Elsevier, Amsterdam (1993)

LAURO-TARONI, L., *et al*., Proc. 21st EPS Conf. on Controlled Fusion and Plasma Physics, Montpellier, **I** (1994) 102

LAWSON, K. D., *et al*., 'An Empirical Method for the Determination of Elemental Components of Radiated Powers and Impurity Concentrations from VUV and XUV Spectral Features in Tokamak Plasmas', Submitted to Physica Scripta (1999)

MAGYAR, G., *et al*., JET Report JET-R(88)15 (1988)

WESSON, J., Tokamaks, (2nd edition), Clarendon, Oxford, (1997) 205